Molecular beam epitaxy growth and characterization of mid-IR type-II "W" diode lasers

C. L. Canedy,[a] W. W. Bewley, G. I. Boishin,[b] C. S. Kim, I. Vurgaftman, M. Kim, J. R. Meyer, and L. J. Whitman
Naval Research Laboratory, Code 5613, 4555 Overlook Avenue, S.W., Washington, DC 20375

(Received 27 October 2004; accepted 20 December 2004; published 7 June 2005)

Type II "W" diodes designed for emission at the spectral line of methane (3.31 μm) when operated near 80 K were grown on a compact 21T RIBER molecular beam epitaxy system. Photoluminescence and cross-sectional scanning tunneling microscopy were used as tools to improve the growth quality of these structures. The diodes exhibited very low lasing thresholds at $T=80$ K (24–40 A/cm^2), although further development will be required to enhance the characteristic temperature ($T_0 \sim 40$ K) and the maximum operating temperature ($\sim$190 K). The lasers had favorable internal losses at all T up to 190 K (~ 7 cm^{-1}), and favorable internal efficiencies at low T (up to 85%). The $I-V$ characteristics of nonlasing test structures were improved substantially by adding n-side "transition" regions that smoothed out abrupt steps in the conduction-band offset. [DOI: 10.1116/1.1861933]

I. INTRODUCTION

In earlier investigations,[1,2] we explored the optimal growth conditions for optically pumped[3,4] mid-IR lasers having the antimonide type-II "W" active region.[5] Some of the conclusions were rather surprising, e.g., that the active-region growth by molecular beam epitaxy (MBE) is most favorable at a much higher temperature (T_{act}) than was employed in virtually all previous fabrications of antimonide W structures.[6–8] Here we report an extension to the case of W diode lasers, which will ultimately be much more practical than optically pumped devices.

Previous W diodes emitting at $\lambda = 3.3$ μm have lased to room temperature when pulsed[9] and to 200 K for cw operation,[10] although those devices were limited by poor current-voltage characteristics. While the electrical properties of subsequent devices (with $\lambda = 3.25-3.56$ μm at the maximum operating temperature) improved somewhat,[11,12] turn-on voltages (V_{th}) were still on the order of 1 V, and T_{max} was only slightly higher for pulsed (220–260 K) than for cw (185–195 K) operation. Interband cascade lasers with 15–25 stages of the W active region have recently lased cw up to 214 K ($\lambda = 3.4$ μm)[13] and 217 K ($\lambda = 3.2$ μm).[14] The cascade devices have displayed voltage efficiencies as high as 96%,[13] i.e., eV_{th} was only slightly larger than the energy gap multiplied by the number of stages. Clearly, single-stage W diodes should similarly benefit from more efficient electrical injection.

Although the strong sensitivity of diode laser performance to growth quality is well known, growth optimization for the antimonide-based systems remains particularly challenging. This challenge applies especially to complicated quantum well (QW) structures such as the W, whose AlGaSb/InAs/GaInSb/InAs active region (in the present structures) incorporates three distinct material systems encompassing a wide range of optimal growth conditions. The difficulty is further magnified by the incorporation of doped cladding layers, separate confinement heterostructure (SCH) regions, hole blocking (HB) regions, and inter-region transition layers that necessitate additional growth-related tradeoffs when the full structure is optimized. To explore some of these issues, in addition to fabricating complete lasers, we also investigated suites of test samples with abbreviated diode structures.

The following approach has been followed in perfecting our growth of these complicated quantum heterostructures at the Naval Research Laboratory (NRL) epicenter. First, growth of the bottom InAs/AlSb superlattice (SL) n clad was enabled. Next the active QW growth was addressed by maximizing the photoluminescence (PL) in a series of samples grown on the n-clad material at a systematically varying range of T_{act}. Then a series of full diodes was grown, for which the AlSb/AlAs p-clad growth temperature was monotonically reduced until no degradation in the structural quality (as determined by high-resolution x-ray diffraction) or PL was observed. Further improvements were deemed necessary based on the unsatisfactory I-V characteristics of the resultant diodes (high V_{th} and series resistance). Hence, a further round of abbreviated test structures was grown with added transition regions on both the n and p side of the active region. These were designed to minimize the formation of electrostatic barriers to carrier transport.

II. EXPERIMENT

The laser diodes were all grown on 2 in. epiready Te-doped GaSb wafers in a compact 21T Riber MBE system equipped with both As and Sb crackers. Growth temperatures were measured using an optical pyrometer sensitive in the 1.5–1.6 μm range, and calibrated using the (1×3) to (1×5) surface reconstruction transition for GaSb ($\sim$429 °C for an Sb_2 flux of 2 ml/s).[15] Growth rates for the group III

[a]Electronic mail: canedy@sisyphus.nrl.navy.mil
[b]Also at NOVA Research Inc., Alexandria, VA 22308.

species were calibrated by using *in situ* reflection high-energy electron diffraction intensity oscillations and the group V valve positions set so as to maintain a V/III flux ratio of 1.5 to 2. Unless otherwise specified the active region comprised five repetitions of 40 Å $Al_{0.35}Ga_{0.65}Sb$/20 Å InAs/30 Å $Ga_{0.92}In_{0.08}Sb$/20 Å InAs, grown with no special shutter sequence at the QW interfaces (mixed interface bond type). This particular W structure was designed for emission at the methane spectral line of 3.31 μm when operated at $T \approx 80$ K. All doping densities were calibrated by growing each individual layer on a 2 μm lattice-matched AlSb/AlAs SL, to electrically isolate it from the *n*-GaSb substrate and buffer layer, and then performing Hall measurements at 300 and 77 K.

Growth of the diode structures began with a 0.4-μm-thick Te-doped ($n \sim 5 \times 10^{17}$ cm^{-3}) GaSb smoothing buffer. This was followed by a 3.3 μm InAs:Si/AlSb SL (24.3 Å/23 Å) *n*-clad layer grown at ~450 °C. Lattice matching to the GaSb substrate was achieved by adjusting the Sb-soak time at both interfaces to accommodate the As incorporation into the AlSb layer. Doping the InAs layers up to within about 1 ML of each interface yielded an effective doping density of 5×10^{17} cm^{-3}. Next, a 0.4-μm-thick Te-doped (2×10^{17} cm^{-3}) GaSb *n*-SCH layer was grown at a temperature of ~490–500 °C. The higher temperature, which helped to provide a smoother surface for the subsequent active-region growth, was found to be critical to maintaining intense PL from the QWs. The SCH layer was followed by a ~47 nm HB layer comprised of an InAs/AlSb SL (24.3 Å/23 Å) grown at $T \sim 480$ °C. In this case the InAs was undoped, in order to reduce free-carrier absorption, and lattice matching was again achieved by adjusting the Sb-soak times at the interfaces. Next came the active QWs, whose optimum growth temperature (T_{act}) was determined by maximizing the PL intensity as discussed below. That was followed by a 0.6-μm-thick undoped $Al_{0.5}Ga_{0.5}As/Al_{0.5}Ga_{0.5}Sb$ SL *p*-SCH layer. The *p*-SCH layer was grown at ~460 °C, the highest of a series of temperatures for which full-diode samples showed no degradation in the structural quality or PL intensity. The thicknesses in this layer were adjusted to achieve lattice matching to the underlying GaSb substrate. Optimization of the growth temperature for the 1.5-μm-thick Be-doped (~5×10^{18} cm^{-3}) AlAs/AlSb *p*-clad layer was performed in the same manner. All samples concluded with a 50 nm Be-doped ($p \sim 5 \times 10^{18}$ cm^{-3}) GaSb cap layer.

Besides the primary functional regions listed in the preceding paragraph, some of the laser and test devices also contained "transition" layers that were designed to smooth abrupt discontinuities in the conduction and valence band profiles at the boundaries between regions. Such discontinuities induce barriers to the electron and hole transport, which can be overcome only by applying additional bias voltage. For example, our baseline diode structure contained several thin (~50 nm) Be-doped $Al_xGa_{1-x}Sb/Al_xGa_{1-x}As$ SL layers between the *p*-SCH and the *p*-clad regions, and also between the *p*-clad and the *p*-cap, to serve as valence-offset-smoothing layers. On the *n* side, all of the devices contained graded, strain-compensated InAs:Si/AlSb SL layers (45–70 nm) between the *n*-GaSb buffer and the *n* clad, and also between the *n*-clad and the *n*-SCH. Subsequently, it was found that additional transition layers consisting of graded GaSb:Te/InAs:Si/AlSb SLs inserted between the *n*-GaSb and the *n*-clad, between the *n*-clad and the *n*-SCH, and between the *n*-SCH and the HB significantly improved the *I-V* characteristics of nonlasing test devices. Unfortunately, the MBE system required venting before that approach could be applied to full laser structures.

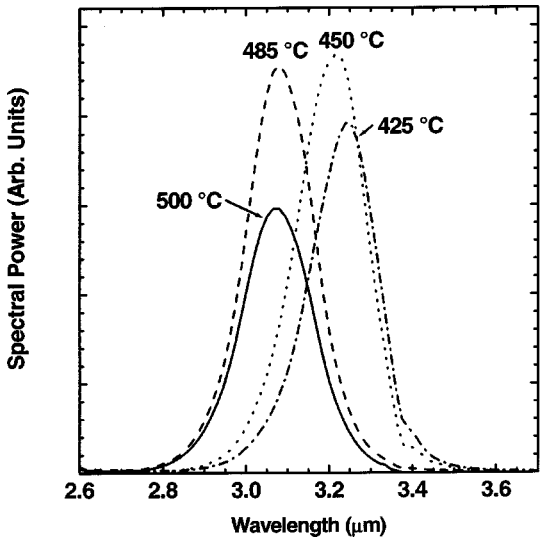

FIG. 1. PL spectra at 78 K for "W" structures with identical five-period active regions [InAs(20 Å)/$Ga_{0.92}In_{0.08}Sb$(30 Å)/InAs(20 Å)/$Al_{0.35}Ga_{0.65}Sb$(40 Å)] and identical growth conditions apart from the indicated substrate temperatures (T_{act}).

III. STRUCTURAL CHARACTERIZATION AND PHOTOLUMINESCENCE

In order to determine the optimal T_{act}, a series of representative test samples was grown and the PL from the W QWs characterized. For those structures, 5 W wells were grown on a HB/*n*-SCH/transition layer/0.5 μm *n*-clad/transition layer/*n*-buffer/*n*-substrate template, and T_{act} was varied from 425 to 500 °C. All layers were grown as in the full laser, except for a thinner *n*-clad. Figure 1 shows the PL intensity as a function of wavelength for the four PL samples with various T_{act}. We see both a shift toward longer wavelengths with increasing T_{act}, and a clear intensity maximum in the 450–480 °C range. An earlier series of W structures (for optical pumping) with AlAsSb digital-alloy barriers displayed similar trends, and an optimal temperature close to 500 °C.[2] In that study the wavelength shift could be attributed to either increased interfacial mixing at the higher temperatures, leading to thinner InAs QWs and a corresponding increase in the electron confinement energy, or a shift in the hole confinement energy induced by In clustering in the GaInSb hole QWs. Cross-sectional scanning tunneling microscopy (X-STM) images confirmed that the trend in the PL intensity resulted from two competing mechanisms: im-

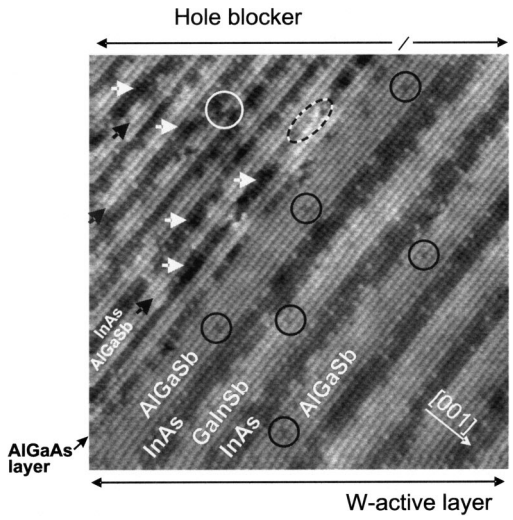

FIG. 2. Filled-states X-STM image of the interface between the HB region ($InAs/Al_{0.7}Ga_{0.3}SbSL$) and the W active region, both grown at 485 °C. The size of the image is 36×36 nm. We have circled background As atoms that incorporated into the Sb-containing layers of the "W" QWs. The black arrows indicate In atoms that diffused into the AlGaSb layers, while the white arrows are Ga or Al atoms that diffused into the InAs layers.

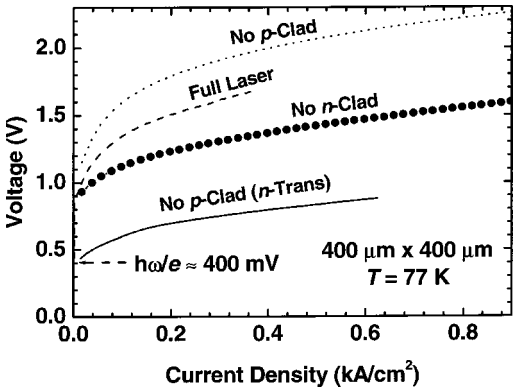

FIG. 3. *I-V* characteristics for test structures with the *n*-clad omitted (curve with points), with the *p* clad and also the active region omitted (dotted), with the *p*-clad omitted and additional transition layers on the *n* side (solid), and the baseline full diode laser (dashed).

proved morphology of the AlAsSb barrier layers at higher T_{act}, combined with reduced In clustering in the GaInSb hole QWs at lower T_{act}. However, the mechanism(s) driving the intensity trend in Fig. 1 may be different, since these structures contain $Al_{0.35}Ga_{0.65}Sb$ rather than AlAsSb barriers, and also less In in the hole QWs (the In/Ga ratio is 0.087 *vs.* 0.43).

We have employed X-STM (Refs. 16 and 17) to view several of the present structures on the atomic scale, although so far no dramatic differences have emerged that could straightforwardly account for the trends in the PL data. A X-STM image for the sample with $T_{act}=485$ °C, in Fig. 2, clearly delineates the HB and active regions. Apart from the background As atoms (circled) within the AlGaSb barriers and GaInSb hole QWs, the W active layers appear to be of high quality. On the other hand, the HB region shows a more substantial group-III interdiffusion, along with group-V exchange (neither of which is necessarily detrimental to the laser performance as long as high crystalline quality is maintained and large-scale nonuniformities do not occur). The Al and/or Ga atoms within the InAs layers are marked with white arrows, while In atoms within the AlGaSb layers are marked with black arrows. We have also identified As-for-Sb and Sb-for-As exchange processes (circled). A noteworthy feature is the emergence of an AlGaAs layer at the boundary between the HB and W regions. This layer forms via the occurrence of As-for-Sb exchange processes during the growth interrupt which must be introduced to prepare the Al and Ga cell temperatures for the active-region growth. By changing the HB to an InAs/AlSb SL, we have since eliminated the need for the growth interrupt, thereby avoiding the formation of this undesirable layer.

IV. TRANSPORT CHARACTERISTICS

A series of test structures was grown to address the unfavorable *I-V* characteristics of the first diode lasers produced in this study (as well as most previously fabricated W diodes[10,11]). In order to understand the origins of the large turn-on voltages and series resistances, we first grew and characterized devices in which one or more region was omitted from the full laser design. This was followed by the fabrication of structures with additional transition layers to minimize discontinuities in the conduction- and valence-band profiles. For these measurements, standard contact photolithography was used to pattern 400 μm $\times$ 400 μm pads on the top *p*-cap layer of the unthinned samples ($\approx$500 μm thick). Each device was then sputter cleaned for 90 s in 20 mTorr Ar^+, at a 400 V dc bias, to remove the oxide layer. Next, 30 nm of Cu was sputter deposited, followed by the deposition of 7.5 nm Cr/100 nm Pt/100 nm Au in an e-beam evaporator. After liftoff, the backside was metallized using a similar process, but with only 5 nm of Cu and 40 nm Sn/100 nm Pt/100 nm Au. The final step was to rapid thermal anneal the device at 300 °C for 1 min.

Figure 3 illustrates *I-V* characteristics at $T=77$ K for three of the samples fabricated in this manner, along with data for a full diode laser (100-μm-wide stripe). The apparent turn-on voltage in a nonlasing diode scales with the reverse saturation current and depends on the scale of the *I-V* plot (here determined by the series resistance), whereas the threshold voltage of an optimized diode laser is very close to the energy gap in the active region ($V_{th}\approx E_g/e\approx400$ mV). The value for the full laser whose characteristics are shown in the figure (dashed curve) is over three times higher. The sources of this excessive V_{th} can be identified with the help of measurements on the partial structures. Note that when the *p*-clad and the active region were omitted (dotted curve), V_{th} actually increased slightly, even though any unwanted electrostatic barriers occurring on the *n*-side would not be altered. However, when the *n*-clad was omitted (curve with points), the apparent turn-on voltage decreased by at least 400 mV compared to the structure with no *p*-clad. We do not

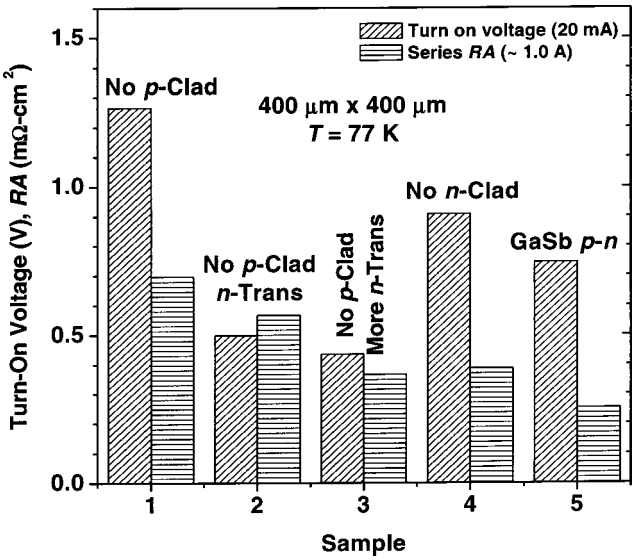

FIG. 4. Bar graph summarizing the *I-V* characteristics at $T=77$ K for five samples from the series of transport test structures. The quantities plotted are turn-on voltage (estimated at $I=20$ mA) and series resistance-area product (estimated from the slope at $I=1$ A), for 400 μm $\times$ 400 μm pads.

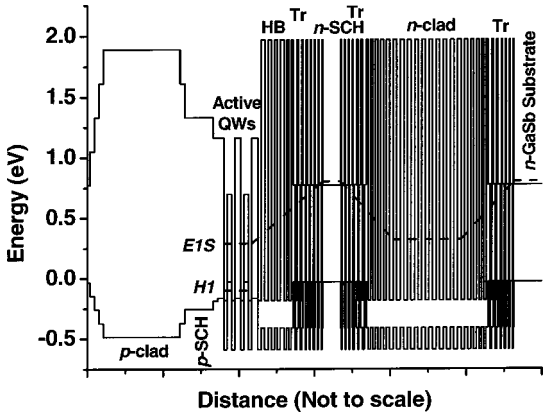

FIG. 5. Conduction and valence band profiles for the full laser structure with transition layers (Tr) on the *n* side. The dashed curve is the profile of the conduction-band ground-state energy level, including quantum confinement but excluding electrostatic fields that almost completely remove the apparent barriers to carrier transport.

expect a decrease to E_g/e in the active region because there was still a large conduction-band discontinuity at the boundary with the *n*-SCH region, which was present in that structure. Results for the device with no *p*-clad and also transition layers on the *n*-side (solid curve) will be discussed below.

The bar graph in Fig. 4 tabulates turn-on voltages required to reach $I=20$ mA and series resistance-area products (RA, as estimated from the *j-V* slopes at $I=1.0$ A), for five different test structures at $T=77$ K. Sample 5 is a simple GaSb *p-n* junction with an apparent turn-on voltage of $\approx$800 mV. The structures with no *p*-clad and on *n*-clad from Fig. 3 are samples 1 and 4, respectively. Not shown is a sample which omitted the *n*-clad as in sample 4, but also included additional *p*-side transition layers to further reduce the valence-band offset steps from those in the baseline structure. Possibly because the growth of the additional AlGaSb/AlGaAs compositions was not fully optimized, the transport in that structure was worse rather than better compared to sample 4. However, the results for sample 2 indicate that the insertion of transition layers between the HB/*n*-SCH, *n*-SCH/*n*-clad, and *n*-clad/substrate boundaries had a very positive effect when the *p*-clad was omitted. It was even more beneficial to expand the transition layers somewhat, to provide even smoother voltage steps. That was done in sample 3 in Fig. 4, whose *I-V* characteristics are also plotted as the solid curve in Fig. 3. For that structure the turn-on voltage approached the laser-threshold limit of $E_g/e\approx 400$ mV. A similar improvement was recently obtained when analogous transition layers were incorporated into W diodes grown at Maxion and designed/characterized at NRL.[18] In pulsed mode, that device operated to 315 K, where the emission wavelength was $\lambda=4.02$ μm.

Figure 5 illustrates the conduction and valence band profiles for all regions of a full laser structure that includes three *n*-side transition layers (Tr), and also a profile of the unperturbed conduction-band ground state (dashed curve) in the absence of any carrier transfer between layers. This figure is schematic since the horizontal coordinate is not drawn to scale (e.g., the two cladding layers should be far thicker relative to the rest of the layers). In the actual doped structure, the graded heterojunctions in Fig. 5 will establish electrostatic fields associated with separation of the electrons from their donors. A self-consistent solution to the one-dimensional Poisson's equation confirms that all of the peaks and valleys in the dashed-curve profile of Fig. 5 are leveled almost completely, from the active region to the *n*-substrate. In other words, no potential barriers remain to impede the electron transport, which is consistent with the experimental finding of a low turn-on voltage for sample 3. On the other hand, internal electrostatic fields are unable to flatten out a more abrupt voltage step (as in sample 1).

While the series resistance data in Fig. 4 are less straightforward to interpret, we simply note that the insertion of transition regions on the *n*-side has a beneficial effect on RA as well. However, we find that even sample 3 has a somewhat higher RA ($\approx$0.37 mΩ cm^2) than the simple GaSb *p-n* junction ($\approx$0.25 mΩ cm^2). One caveat is that current spreading affects the resistances measured for the 400 μm $\times$ 400 μm pad areas and $\approx$500 μm thicknesses of the test devices. A second caveat is the uncertain role of contact resistance, which is still under investigation. We finally note the *I-V* characterizations at $T=300$ K yielded qualitatively similar results with generally lower turn-on voltages, which reflects stronger carrier diffusion as well as the mitigation of the detrimental effects of band-offset discontinuities by the higher thermal energy. Again, it has not yet been possible to fabricate full laser diodes that take advantage of the improved transport associated with *n*-side transition layers.

V. LASING CHARACTERISTICS

Diode lasers were prepared by first sputter-cleaning with Ar^+ to improve adhesion and then depositing 130 nm of

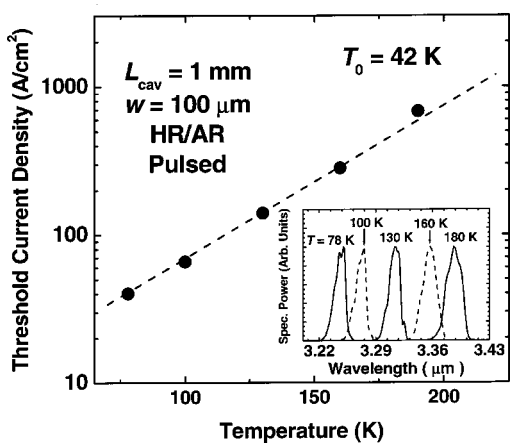

FIG. 6. Pulsed threshold current density vs temperature for a pulsed W diode laser with 5 QWs. The cavity length is 1 mm, the stripe width is 100 μm, and both facets are coated (HR/AR). The inset shows spectra taken at five different temperatures for a sister device with L_{cav}=2 mm.

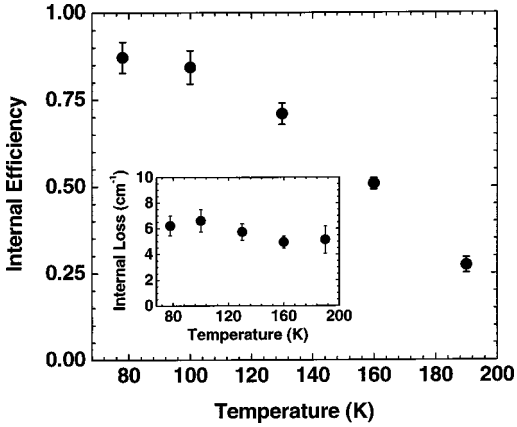

FIG. 7. Internal loss and internal efficiency as a function of temperature as determined by a cavity length study of the inverse efficiency.

SiO_2. Next, 100-μm-wide stripes were defined by photolithography and etch back and dice points defined. The *p*-side metallization proceeded as detailed above and the samples were thinned to ~150 μm. The backside was then metallized and the samples annealed as before. Laser cavities of various lengths were defined by cleaving. Some lasers had coated facets, which were e-beam evaporated (~515 nm Al_2O_3 for AR and 50 nm Al_2O_3/100 nm Au/50 nm Al_2O_3 for HR).

Figure 6 plots the pulsed threshold current density *vs.* temperature for a device with five QWs. The pulse length was 250 ns at a repetition rate of 50 Hz. Despite the low threshold current density of 40 A/cm^2 at T=78 K (a sister device had an even lower threshold of only 24 A/cm^2 at 78 K), the characteristic temperature was also low (T_0 =42 K). This led to poor performance at higher temperatures, and a maximum pulsed operating temperature of 190 K. The inset shows spectral data for a sister laser at five different temperatures. The linewidths are ~15 nm, and the peak shifts from 3.25 to 3.39 μm as the temperature is increased from 78 to 180 K, due primarily to the decrease of the energy gap.

A study of the external quantum efficiency at a series of cavity lengths yielded both the internal loss and the internal efficiency. Figure 7 illustrates results as a function of temperature. The internal loss, which is probably due primarily to intervalence resonances, maintains a constant value of ~7 cm^{-1} up to the highest operating temperature of 190 K. In contrast, the internal efficiency is quite good at low T (85% at 78 K), but decreases rapidly with increasing temperature. The reasons for this precipitous drop are still under investigation. We note that the slope efficiency of 186 mW/A measured for a 1-mm cavity with coated facets at T=78 K (not shown) corresponds to an external quantum efficiency of 49%, which is higher than any earlier result we are aware of at this wavelength.

VI. SUMMARY

We have made substantial progress toward optimizing the MBE growth of antimonide type-II W diode lasers emitting at $\lambda \approx 3.2-3.4$ μm. The optimal temperature window for growth of the active layers is determined to be 450–480 °C. Transport studies show that it is highly desirable to include transition layers to smooth out the band offset discontinuities on the *n*-side. The diodes grown so far have very promising low-T characteristics, although they unfortunately degrade relatively rapidly with increasing temperature.

ACKNOWLEDGMENT

This work was supported by the Office of Naval Research.

[1]C. L. Canedy, W. W. Bewley, C. S. Kim, M. Kim, I. Vurgaftman, and J. R. Meyer, J. Appl. Phys. **94**, 1347 (2003).
[2]C. L. Canedy, G. I. Boishin, W. W. Bewley, C. S. Kim, I. Vurgaftman, M. Kim, J. R. Lindle, J. R. Meyer, and L. J. Whitman, J. Vac. Sci. Technol. B **22**, 1575 (2004).
[3]W. W. Bewley, C. L. Felix, I. Vurgaftman, D. W. Stokes, E. H. Aifer, L. J. Olafsen, J. R. Meyer, M. J. Yang, B. V. Shanabrook, H. Lee, R. U. Martinelli, and A. R. Sugg, Appl. Phys. Lett. **74**, 1075 (1999).
[4]R. Kaspi, A. P. Ongstad, G. C. Dente, J. Chavez, M. L. Tilton, and D. Gianardi, Appl. Phys. Lett. **81**, 406 (2002).
[5]J. R. Meyer, C. A. Hoffman, F. J. Bartoli, and L. R. Ram-Mohan, Appl. Phys. Lett. **67**, 757 (1995).
[6]M. J. Yang, W. J. Moore, C. H. Yang, R. A. Wilson, B. R. Bennett, and B. V. Shanabrook, J. Appl. Phys. **85**, 6632 (1999).
[7]M. J. Yang, W. J. Moore, B. R. Bennett, B. V. Shanabrook, J. O. Cross, W. W. Bewley, C. L. Felix, I. Vurgaftman, and J. R. Meyer, J. Appl. Phys. **86**, 1796 (1999).
[8]R. Kaspi, A. P. Ongstad, G. C. Dente, J. Chavez, M. L. Tilton, and D. Gianardi, Appl. Phys. Lett. **81**, 406 (2002).
[9]H. Lee, L. J. Olafsen, R. J. Menna, W. W. Bewley, R. U. Martinelli, I. Vurgaftman, D. Z. Garbuzov, C. L. Felix, M. Maiorov, J. R. Meyer, J. C. Connolly, A. R. Sugg, and G. H. Olsen, Electron. Lett. **35**, 1743 (1999).
[10]W. W. Bewley, H. Lee, I. Vurgaftman, R. J. Menna, C. L. Felix, R. U. Martinelli, D. W. Stokes, D. Z. Garbuzov, J. R. Meyer, M. Maiorov, J. C. Connolly, A. R. Sugg, and G. H. Olsen, Appl. Phys. Lett. **76**, 256 (2000); unpublished data.
[11]M. Kim, W. W. Bewley, J. R. Lindle, C. S. Kim, I. Vurgaftman, J. R. Meyer, J. G. Kim, and R. U. Martinelli, Appl. Phys. Lett. **83**, 5374 (2003).
[12]C. Mermelstein, J. Schmitz, R. Kiefer, M. Walther, and J. Wagner, Appl. Phys. Lett. **85**, 537 (2004).

[13]J. L. Bradshaw, N. P. Breznay, J. D. Bruno, J. M. Gomes, J. T. Pham, F. J. Towner, D. E. Wortman, R. L. Tober, C. J. Monroy, and K. A. Olver, Photonics Spectra **20**, 479 (2004).
[14]R. Q. Yang, C. J. Hill, L. E. Christensen, and C. R. Webster, Proc. SPIE (to be published).
[15]A. S. Bracker, M. J. Yang, B. R. Bennett, J. C. Culbertson, and W. J. Moore, J. Cryst. Growth **220**, 384 (2000).
[16]S. G. Kim, S. C. Erwin, B. Z. Nosho, and L. J. Whitman, Phys. Rev. B **67**, 121306 (2003).
[17]B. Z. Nosho, W. Barvosa-Carter, M. J. Yang, B. R. Bennett, and L. J. Whitman, Surf. Sci. **465**, 361 (2000).
[18]W. W. Bewley, I. Vurgaftman, C. S. Kim, M. Kim, C. L. Canedy, J. R. Meyer, J. D. Bruno, and F. J. Towner, Appl. Phys. Lett. **85**, 5544 (2004).